PHASE-TRANSITION PROCESS IN THE HYDROTHERMAL ZEOLITIZATION OF VOLCANIC ASH INTO LTA AND FAU STRUCTURES

Jorge D. Monzón[1], Maximiliano R. Gonzalez[1]* (iD), Mercedes Muñoz[1], Andrea M. Pereyra[1,2], and Elena I. Basaldella[1]

[1]Centro de Investigación y Desarrollo en Ciencias Aplicadas Dr. J.J. Ronco (CINDECA) (CONICET-CIC-UNLP), 47 N°257, B1900 AJK La Plata, Argentina
[2]Universidad Tecnológica Nacional - Facultad Regional La Plata, 60 y 124, 1900 La Plata, Argentina

Abstract—Minerals such as quartz, present widely in various volcanic ashes, remain unaltered throughout the low-temperature hydrothermal process currently used in industry to obtain zeolites, causing an incomplete hydrothermal transformation of the starting solid. This study presents a novel and cost-effective procedure which improves the reactivity of ash toward the generation of zeolite by increasing the availability of silica and alumina components. This method leads to a final product with a large zeolite content. The transformation consisted of an ash-activation step followed by hydrothermal zeolitization. The influence of the structural, chemical, and morphological characteristics of the volcanic ash as well as the effect of the activation procedure on the ash reactivity were studied. A collected sample (VA) and an amorphous fraction obtained after VA sieving (VA40, retained on #40 mesh) were used for zeolite production. These solids were alkaline-treated separately, aged, and reacted under controlled conditions of temperature at autogenous pressure. Throughout the process, the solid phases were characterized by X-ray diffraction, energy dispersive X-ray microanalysis, scanning electron microscopy, Fourier-transform infrared spectroscopy, and N_2 adsorption-desorption porosimetry measurements. After activation and alkaline aging, the presence of quartz and plagioclase minerals in the natural ash seemed to improve the growth of $NaAlSiO_4$ polymorphs, which in turn were transformed easily to zeolite structures. Even under adequate pretreatment and suitable synthesis conditions, the coarse non-crystalline fraction led to low conversion, while the highest conversions to zeolites A and X were obtained from the natural ash. The outcomes of the present study could be used to improve the conversion levels of other non-conventional aluminosiliceous minerals into zeolites.

Keywords—Alkaline pretreatment · Hydrothermal synthesis · Mineralogical and chemical composition · $NaAlSiO_4$ polymorphs · Volcanic ash · Zeolites

INTRODUCTION

Volcanic ash includes pyroclastic material with a particle size of <2 mm, which is formed during volcanic eruptions. The violent nature of eruptions causes the magma and solid rocks to separate into these tiny particles and other larger materials (>2 mm) such as volcanic scum and pumice (Lemougna et al., 2018).

After decades of quiescence, the Puyehue-Cordón Caulle volcanic complex (PCCVC; Chile) erupted in 2011. As usual in Andean eruptions (Folch et al., 2008), the dominant regional winds drove the ash clouds over the Andes and caused abundant ash fallout in the south of Argentina, also affecting the proximal Chilean areas. This event was significant and the transport and deposition of ash as well as its detrimental effects on the spread area were studied intensively (Collini et al., 2013; Klüser et al., 2013; Elissondo et al., 2016).

Volcanic ashes are harmful materials for the environment and human health (Covey et al., 2021), impacting negatively on socio-economic development (Wilson et al., 2011). Due to the wind, the process of mobilization and atmospheric re-suspension is one of the most important factors in determining the seriousness of risks (Wilson et al., 2011).

The chemical composition and structural properties of volcanic residues make them suitable for technological applications. The literature reports engineering applications such as: filler for roadway and pavement material (Gautam et al., 2018); cement replacement (Siddique, 2011; Al-Fadala et al., 2017); geopolymers (Lemougna et al., 2011; Tchakoute Kouamo et al., 2012; Tchakoute et al., 2013); adsorbent for pollutants (Botto et al., 2013); catalysis (Muñoz et al., 2019), among others.

The presence of inorganic compounds, such as amorphous silicates or aluminosilicates (Botto et al., 2013); and some crystalline phases (particularly plagioclase) (Canafoglia et al., 2012), allows their use as raw material in the synthesis of zeolites. The zeolitization process without an appropriate activation of the starting solid produces a final product within which quartz remains (Sanhueza Nuñez & Bennun Torres, 2015). As a consequence, an activation that includes calcination in the presence of various alkali sources is suitable. An alkaline fusion method with NaOH as pretreatment was used (Lee et al., 2018; Belviso et al., 2021), but the published results involve some drawbacks such as hard-cake products, low zeolite conversions, or the co-crystallization of different zeolite structures.

* E-mail address of corresponding author: maximi_gonz@yahoo.com.ar

A great variety of raw materials used for the synthesis of zeolites can be found in the literature. They include low-cost natural materials such as clay minerals (Gougazeh et al., 2019; Chen et al., 2020) and waste generated by the energy industry or agriculture (Mohamed et al., 2015; He et al., 2020).

Concerning waste reutilization, previous studies (Gonzalez et al., 2016; Monzón et al., 2017) focused on the conversion of aluminosiliceous residues (exhausted catalysts and fly ash) into zeolite A, a material used widely in technological processes such as adsorption and cation exchange. The procedure for obtaining A-type zeolite from these wastes involves a suitable alkali activation with Na_2CO_3 followed by hydrothermal synthesis. Results have shown that pretreatment conditions which favor the generation of crystalline nepheline and low-carnegieite, two polymorphic forms of $NaAlSiO_4$, are beneficial for obtaining large amounts of zeolite A after synthesis, attaining a conversion of close to 80%.

Some siliceous compounds such as quartz, present commonly in the ash, do not react under the usual synthesis conditions used in the industry for producing low-silica zeolites. The aim of the present study was to achieve efficient transformation of a residual volcanic ash into a product containing A-type(LTA) and X-type(FAU) zeolites, free of other crystalline impurities, avoiding the need for using extended reaction times or more exigent synthesis conditions for a complete hydrothermal transformation.

EXPERIMENTAL

Materials

Volcanic ash (VA) from the Puyehue-Cordón Caulle (volcanic complex located in Chile) was used as a raw material. This pyroclastic material belonged to the June 2011 eruption. The ash sample was collected at Bariloche, Río Negro, Argentina (91 km from the volcanic complex, 41°09′S 71°18′W).

The natural material was suspended in distilled water under stirring for 72 h at room temperature and dried for 24 h at 60°C. The VA was then sieved (#40 mesh), and the >0.425 mm particle-size fraction was separated from the bulk (VA40). The chemical compositions of samples VA and VA40 were obtained by energy dispersive X-ray microanalysis (EDX).

Activation Pretreatments and Hydrothermal Synthesis

Before the hydrothermal step, samples VA and VA40 were activated by either alkaline fusion or by milling amorphization in order to enhance their reactivity toward zeolite crystallization. Both procedures had been tested in previous work (Gonzalez et al., 2016; Monzón et al., 2017). For alkaline activation, a mixture containing equal amounts of VA and analytical-grade Na_2CO_3 (J.T. Baker, Phillipsburg, New Jersey, USA) was sonicated for 300 s in order to obtain an homogeneous sample (Monzón et al., 2017). Then, the mixture was calcined under static conditions at 800°C (5°C·min^{-1}) for the selected time. The same procedure was applied to sample VA40. The activated samples were named VA_C and $VA40_C$. To activate the samples by milling (VA_M and $VA40_M$), VA and VA40 were submitted to milling for 60 min, in a Herzog

HSM 100 (HERZOG Maschinenfabrik GmbH, Osnabrück, Germany) oscillating mill.

Subsequently, each sample was placed in contact with the synthesis solution in a 250 mL polypropylene reactor. The synthesis solution consisted of appropriate amounts of NaOH (CARLO ERBA Reagents, Paris, France) and deionized water; $NaAlO_2$ commercial solution (36.5% Al_2O_3, 29.6% Na_2O, 33.9% H_2O) (ALUM, Buenos Aires, Argentina) was added as an extra aluminum source at the beginning of the synthesis in order to obtain the selected starting molar ratios for producing NaA or NaX zeolite as the main product. Each sample was mixed with a magnetic stirrer for 30 min and aged at room temperature for the indicated time (Table 1). The mixture was then placed in a conventional air oven at 100°C.

The course of the reaction was followed by taking aliquots after 0, 3, 6, and 24 h. The solid products obtained were washed and dried in a conventional air oven at 110°C.

Different hydrothermal products were obtained by varying the activation-step conditions and aging times (Table 1).

Physicochemical Characterization

The structural characterization of crystalline materials (starting volcanic ash, the products obtained after pretreatment, and those resulting from hydrothermal synthesis) was carried out by XRD. The diffraction patterns were obtained using a PANalytical X′Pert PRO 3373/00 instrument (PANalytical B.V., Almelo, The Netherlands) (40 kV, 40 mA, CuKα with Ni filter, step size 0.02°2θ). The types of zeolite and other crystalline phases obtained were determined by comparing diffraction profiles with published data (PDF, Powder Diffraction File). The Rietveld method (Rietveld, 1969) and the *FULLPROF* program (Rodríguez-Carvajal, 2001) were used for the quantitative determination of the crystalline components of VA using a PANalytical X′Pert 3020 instrument (PANalytical B.V., Almelo, The Netherlands) (35 kV, 40 mA, CuKα radiation, and Ni filter). A Bruker IFS 66 (Bruker Optik GmbH, Ettlingen, Germany) FTIR spectrophotometer was used to record infrared spectra in the 400–4000 cm^{-1} range. The samples were prepared by dilution in KBr (100 mg KBr/1 mg zeolite sample). Then, the mixtures were subjected to high pressure in a sample holder in order to form pellets. The morphology and semiquantitative chemical compositions of the solid samples were determined by scanning electron microscopy (SEM) using a Philips 505 microscope (Philips, Eindhoven, The Netherlands) equipped with an EDX Prime 10 spectrometer.

N_2 adsorption-desorption isotherms were obtained using a Micromeritics ASAP 2020 automated gas adsorption system (Micromeritics Instrument Corporation, Norcross, Georgia, USA) at the temperature of liquid nitrogen (–196°C) in a relative pressure (p/p_0) range of 0.01–0.99. Before adsorption, samples were out-gassed by heating at 350°C in vacuum, with a pressure of $<3\times10^{-2}$ mm Hg for 12 h. The specific surface area was estimated by the Brunauer Emmett Teller (BET) method (Brunauer et al., 1938), the micropore and the external surface area were determined using the t-plot method (Gregg &

Table 1. Identification of products, starting solids, pretreatment procedures, synthesis mixture type, and aging times used

Product	Starting solid	Milling	Alkaline fusion			Synthesis mixture type	Aging time (h)
		Milling time (min)	Ash/carbonate ratio (w/w)	Temperature (°C)	Fusion time (h)		
$VA_{CZ}1$	VA_C		1	800	12	X	48
$VA_{CZ}2$	VA_C	–	1	800	12	A	48
VA_Z1	VA	No pretreatment				X	48
VA_Z2	VA	No pretreatment				A	48
VA_{MZ}	VA_M	60				X	96
$VA40_{CZ}1$	$VA40_C$	–	1	800	12	A	48
$VA40_{CZ}2$	$VA40_C$	–	1	800	24	A	48
$VA40_{MCZ}1$	$VA40_{MC}$	60	1	800	12	A	48
$VA40_{MCZ}2$	$VA40_{MC}$	60	1	800	24	A	48

Sing, 1982), and the pore-size distribution was evaluated by the Horvath-Kawazoe method (Horvath & Kawazoe, 1983).

Zeolite Conversions

The zeolite content of the samples obtained was calculated by XRD. The relative crystallinity was estimated by the intensity of the characteristic diffraction peaks. These intensities were compared with those present in the pattern of a pure zeolite sample synthesized in the laboratory, which was set to be 100%. The crystallinity was obtained by comparing the intensities of the peaks assigned to the three main reflections, based on ASTM D5357-19 and D3906-19 test methods for zeolites A and X, respectively.

RESULTS AND DISCUSSION

Chemical Analysis

The chemical composition and the SiO_2/Al_2O_3 wt.% ratio were obtained by EDX for VA and V40 (Table 2). The chemical compositions for both samples were very similar, but the amount of Fe_2O_3 (present as magnetite structure in the ash) was greater for VA40. The SiO_2/Al_2O_3 wt.% ratio was slightly higher for natural volcanic ash (VA).

According to the SiO_2/Al_2O_3 ratio obtained for each sample, the amounts of Al_2O_3, Na_2O, and H_2O in the synthesis mixture were adjusted in order to obtain the zeolite desired (A or X type). The starting molar ratios (including the theoretical values provided by the volcanic ash) used for synthesizing zeolite X were $SiO_2/Al_2O_3 = 6$, $Na_2O/H_2O = 0.03$, and $Na_2O/Al_2O_3 = 9.8$. For zeolite A, the molar ratios were $SiO_2/Al_2O_3 = 1.4$, $Na_2O/H_2O = 0.03$, and $Na_2O/Al_2O_3 = 3.4$. The two starting mixtures were named types X and A, respectively (Table 1).

Mineralogical Analysis of the Fly Ash

According to the XRD analysis for VA and VA40 (Fig. 1), the mineralogical composition of volcanic ash depended on the particle-size distribution of the sample studied. The natural volcanic ash, sample VA, contained crystalline and amorphous

fractions, identified by applying the Rietveld method (Fig. 1). The data collected indicated the presence of quartz (PDF# 85-0457, SiO_2), andesine (PDF# 83-1938, $Na_{0.622}$ $Ca_{0.368}Al_{1.29}Si_{2.71}O_8$), and a wide amorphous halo in the angular region 17 to 35°2θ, centered at ~24°2θ. Andesine is a solid isomorphic solution composed of 70–50% albite ($NaAlSi_3O_8$) and 30–50% anorthite ($CaAl_2Si_2O_8$) (Jiménez-Alvarez & Téllez-Jurado, 2010). The potassium detected by EDX could be located in the crystalline network of albite, replacing some Na ions. Small peaks of calcite (PDF# 72-1650, $CaCO_3$) and magnetite (PDF# 86-1351, $Fe_{2.936}O_4$) were also detected in the ash pattern.

Regarding the VA40 fraction, the X-ray diffraction (XRD) pattern presented purely disordered characteristics. The VA40 pattern showed the wide amorphous halo in the same angular region as observed for the VA diffraction pattern (Fig. 1).

Phase Transformation after Pretreatments

The structural transformations throughout the synthesis process was followed by XRD (Fig. 2). After the alkaline fusion activation step of VA, the XRD revealed a change in the structural composition (VA_c). The crystalline phases originally present in the volcanic ash disappeared (mainly quartz and andesine), and new crystalline compounds associated with $NaAlSiO_4$ grew. The new phases were identified by the (International Center for Diffraction Data Powder Diffraction File) PDF# 19-1176, ascribed to nepheline, and PDF# 11-0221, assigned to low-carnegieite. Sodium carbonate was also found. The activation process generated significant levels of both polymorphs, accompanied by a decrease and a clear shift in the amorphous phase from 20–30°2θ to 25–35°2θ (Fig. 2, curve b). The generation of the same $NaAlSiO_4$ polymorphic structures had already been noted in a previous study (Gonzalez et al., 2016; Monzón et al., 2017) where residual catalyst and fly ash were zeolitized.

The sodium carbonate pretreatment thus led to the dissolution of sodium and calcium plagioclase (albite and anorthite, respectively), quartz, as well as the minor phases present in the volcanic ash (magnetite and calcite). The transformation

Table 2. Chemical composition of VA and VA40

Sample	Compound (wt.%)						SiO_2/Al_2O_3 wt. ratio
	Na_2O	Al_2O_3	SiO_2	K_2O	CaO	Fe_2O_3	
VA	4.57	14.11	73.95	2.01	1.51	3.85	5.24
VA40	4.86	14.17	71.47	2.33	1.73	5.44	5.04

involved two mechanisms that appear simultaneously: (1) the displacement of Ca^{2+} ions (provided by anorthite and partially substituted albite) and K^+ ions (from the partially substituted albite) by Na^+ ions of the fluid phase (Na_2CO_3); and (2) the release of Al and Si from the breakdown of andesine and quartz, which combine with Na^+ from the fluid to generate $NaAlSiO_4$ polymorphs. The following equation describes the reaction that controls the process in the case of the calcium endmember of plagioclase (anorthite): $CaAl_2Si_2O_8 + 2Na^+ = 2NaAlSiO_4 + Ca^{2+}$ (Rao and Murthy, 1974). A similar mechanism could be proposed for albite, and the albite partially substituted by K^+ ions. These results showed the transformation of tectosilicate structures (continuous framework of tetrahedra, each sharing all four oxygen atoms: $(SiO_2)_n$ as quartz, K-feldspar, andesine, Si:O ratio 1:2) into $NaAlSiO_4$ polymorphs by a fluid-mediated reaction that involved the dissolution of the original crystalline compounds, accompanied by the precipitation of the new polymorphic phases. In this transformation, the fluid phase promotes the reacting mineral conversion into a mixture of amorphous and crystalline phases (Hamilton et al., 2001; Upadhyay, 2012; Crundwell, 2014).

Subsequently, some additional restructuring occurred during the aging period, noted by comparison of the respective

XRD patterns. At the end of the aging period, a crystalline equilibrium seemed to be attained between the two main polymorphs, the nepheline was dissolved partially and the diffraction patterns showed the peaks of low-carnegieite and small intensities of the remaining nepheline (Fig. 2, curve c).

Similar behavior was noted for the XRD evolution recorded for sample VA40 (Fig. 3). Nevertheless, the peak intensities of $NaAlSiO_4$ polymorphs obtained after alkaline fusion (Fig. 3, curve b) were noticeably smaller than those present in the pattern of VA_C treated for 12 h. Thus, the reactivity toward the polymorph crystallization depended on the mineralogical composition of the starting ash sample.

After aging, VA_C and $VA40_C$ showed the presence of nepheline and low-carnegieite. In both samples, the nepheline was dissolved preferentially (Fig. 2, curve c and Fig. 3, curve c). The greatest peak intensities corresponding to the polymorphs were found in the $VA40_C$ pattern (Fig. 3, curve c). The milled samples (VA_{MC} and $VA40_{MC}$) showed an increased degree of amorphousness after pretreatment, and the polymorphic peak intensities were smallest.

With respect to $NaAlSiO_4$-polymorph generation, the alkaline pretreatment applied to the non-crystalline ash fraction VA40 involved a similar route to that described for VA: the dissolution of amorphous aluminosilicates took place during alkaline fusion, followed by the polymerization of active groups to form three-dimensional networks made of various units of connected SiO_4 and AlO_4 tetrahedra, and the incorporation of Na^+ as compensation ions (Tait et al., 2003; Kumar et al., 2014).

Hydrothermal Synthesis

According to the reaction conditions, different zeolite structures and conversion levels were obtained (Table 3).

VA zeolitization – Zeolite X. The zeolitization of VA using the synthesis mixture composition X was evaluated after 24 h of reaction. For this sample the greatest degree of conversion to zeolite X was obtained (72% of zeolite X, Table 3, $VA_{CZ}1$). The XRD pattern (Fig. 2, curve c) corroborates the transformation VA → $VA_{CZ}1$.

On the other hand, according to the XRD results, the synthesis composition was adjusted to obtain zeolite X from VA samples aged for 48 h and 96 h without alkaline activation mainly produced zeolite P (synthetic zeolite analogue of the gismondine-like framework). Small peaks corresponding to andesine were still observed after 3 h of synthesis time in both samples. After 6 h of reaction, andesine crystals disappeared completely, and a product containing 10% of zeolite A and
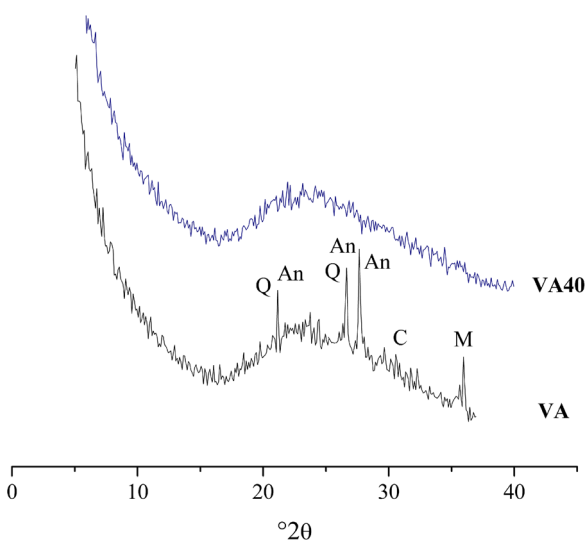
Fig. 1. XRD pattern of natural volcanic ash (VA) and of a volcanic ash particle-size fraction >0.425 mm (VA40). Quartz (Q), andesine (An), magnetite (M), and calcite (C)
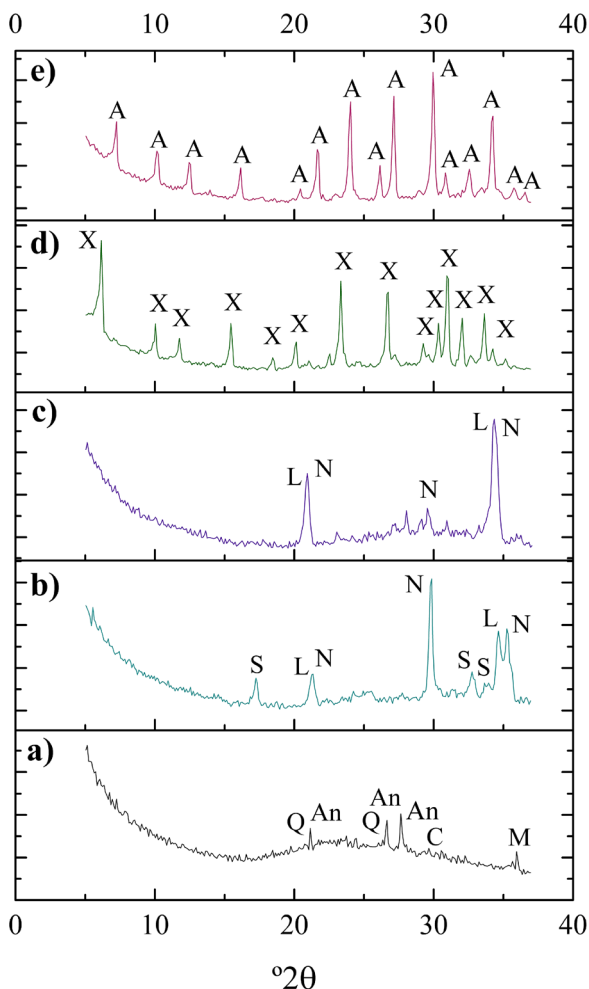
Fig. 2. Evolution of the XRD patterns during zeolite synthesis from VA. **a** VA, **b** VA_C (12 h at 800°C), **c** VA_C after aging at room temperature (48 h), **d** product after zeolite X crystallization, and **e** product after zeolite A crystallization. Quartz (Q), andesine (An), magnetite (M), calcite (C), low-carnegieite (L), nepheline (N), sodium carbonate (S), zeolite X (X), and zeolite A (A)

60% of zeolite P was obtained in both reactions (Table 3, samples VA_Z1 and VA_{ZM}).

Zeolite A. As expected, the synthesis mixture prepared using VA_C and aged for 48 h produced zeolite A (Table 3, sample $VA_{CZ}2$). In this experiment, the diffraction pattern obtained after 3 h of reaction showed clear, high-intensity peaks of zeolite A (Fig. 2, curve e). Thus, 88% conversion to zeolite was obtained after 3 h of reaction.

Synthesis using the composition adjusted to obtain zeolite A from the natural, non-pretreated VA sample, aged for 48 h (Table 3, sample VA_Z2) showed hydroxysodalite after 3 h of reaction. Small peaks related to andesine were also detected in the diffraction pattern (not shown). At longer reaction times, andesine disappeared, and the intensities of the hydroxysodalite (HS) zeolite peaks increased.

V40 Zeolitization. The batch used to synthesize NaA using the amorphous fraction VA40 was also adjusted considering that the SiO_2, Al_2O_3, and Na_2O amounts provided by the ash reacted fully in the hydrothermal conversion.

As mentioned previously, the XRD patterns for samples $VA40_{CZ}1$, $VA40_{CZ}2$, $VA40_{MCZ}1$, and $VA40_{MCZ}2$ corroborated that after alkaline pretreatment for 12 h ($VA40_{CZ}1$), or 24 h ($VA40_{CZ}2$), the peak intensities of $NaAlSiO_4$ polymorphs at the end of the aging time were smaller than those obtained starting from VA. Similar results were found when additional milling for 1 h was included ($VA40_{MCZ}1$ and $VA40_{MCZ}2$). The conversions in zeolite A were also very low, ~20–25% (Table 3). This fact confirms that the presence of polymorphic species at the beginning of the hydrothermal crystallization is beneficial for zeolite growth. Besides, 1 h of milling treatment did not alter meaningfully the conversion level attained. These results are in agreement with previous work (Yamada et al., 2018), where the generation of zeolitic arrangements depended on the crystalline ordering of the precursor phase.

The mechanism of topotactic transformation of polymorphic species into zeolitic structures could be explained on the basis of the three-dimensional reorganization and reconnection of building units occurring when the reacting solid phase is energetically disturbed. As reported (Baerlocher et al., 2007), similar composite building units (CBUs) and secondary building units (SBUs) are common for the wide variety of aluminosiliceous materials. The planar SBUs are also capable of reorganizing themselves to form a three-dimensional structure after specific activation procedures. The planar arrangements of rings, such as the single six-membered ring (S6R) present in $NaAlSiO_4$ polymorphs, can be folded into an α-cage by thermal treatment (Boscoboinik et al., 2013). In the current study, in addition to heat treatment, the chemical composition was adjusted in terms of the Si/Al ratio to lead the reaction toward the intended zeolitic structure. The feasibility of this rearrangement was reinforced by the fact that it could be reversed under selected working conditions. According to the literature (Lutz et al., 1985; Dimitrijevic et al., 2004), temperatures >700°C led to the destruction of the initial zeolite framework, by D4R rings breaking and the unfolding of the supercage into a planar structure of S6R tetrahedral building units. Polymorphic $NaAlSiO_4$ frameworks were reconstituted by forming and connecting the S6R member rings, the Si^{4+} and Al^{3+} cations being ordered to obey Loewenstein's rule. On the other hand, following the inverse transformation, the lack of the LTA and FAU zeolitic ordering toward low-carnegieite and pure sodium nepheline growth, induced by heating, has also been reported (Dimitrijevic et al., 2004).

Comparing the XRD peaks present in the patterns obtained from the solid phases VA_C and $VA40_C$ after 48 h of aging, the generation of the two polymorphs (nepheline and low-carnegieite) was observed, the crystallization being more pronounced starting from VA_C. This fact, along with the displacement of the amorphous halo detected after the pretreatment, confirms that zeolite crystallization depends not only on the
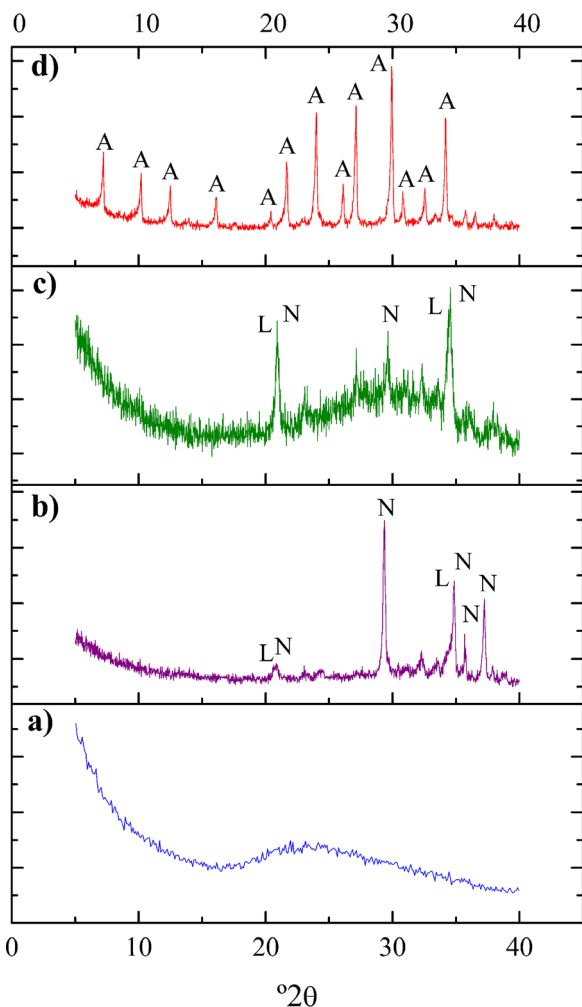
Fig. 3. Evolution of the XRD patterns during zeolite synthesis from the VA40 fraction. **a** VA40, **b** VA40$_C$ (12 h at 800°C), **c** VA40$_C$ after aging at room temperature (48 h), and **d** product after zeolite A crystallization. Low-carnegieite (L), nepheline (N), and zeolite A (A)

chemical composition of the raw material but also on the presence of the polymorphs. Despite the similar chemical composition of VA and VA40 and equal pretreatment conditions applied to both samples, differences in zeolite content were detected when comparing the zeolitized VA$_{CZ}$ and VA40$_{CZ}$ products.

In addition, with respect to the amorphous component, non-crystalline materials can be considered less susceptible to transformation into zeolite than crystalline precursors (Yamada et al., 2018). This can be attributed to the presence of Al–O–Al bonding, which is forbidden in the framework of zeolites, mainly when the Si/Al ratio is 1.0 (zeolites A and X) (Loewenstein, 1954). The existing differences between the amorphous/crystalline samples in VA$_Z$ and VA40$_Z$ could also be correlated with the different zeolite crystallization level, estimated when comparing VA$_Z$ and VA40$_Z$.

FTIR Analyses

The volcanic ash, pure zeolites (A and X), and the zeolites obtained from the volcanic ash (VA$_{CZ}$1 and VA$_{CZ}$2) were studied by Fourier-transform infrared (FTIR) analysis in the frequency range 400 to 4000 cm^{-1} (Fig. 4).

For all samples, the recorded IR spectra showed signals corresponding to adsorbed water, indicated by the dominant O–H stretching signal at ~3450 cm^{-1}. In addition, the peak at ~1650 cm^{-1}, characteristic of the bending mode in the water molecule (δH–O–H bond), was observed clearly (Fig. 4a). These bands were more attenuated in the volcanic ash spectrum (Fig. 4a.I), indicating an increased presence of water molecules in the more open zeolitic structures.

Regarding the volcanic ash, the characteristic signals of its aluminosiliceous composition were detected (Hamilton et al., 2001) (Fig. 4b.I). The signals corresponding to the symmetric and asymmetric stretching vibrations (ν_{as} and ν_s) of T–O (T = Si, Al) were observed in the tetrahedral environment at 1050–1100 and 790 cm^{-1}, respectively, and the network stretching modes at ~460 cm^{-1}.

After synthesis, the structural zone spectra (exhibited at wavenumber values of <1200 cm^{-1}) of the zeolitized volcanic ash (VA$_{CZ}$1, Fig. 4b.III, and VA$_{CZ}$2, Fig. 4b.V) were coincident with the spectra of their pristine zeolites (Fig. 4b.II and Fig. 4b.IV).

Thus, the IR spectra of both zeolite X and VA$_{CZ}$1 (Fig. 4b.II and Fig. 4b.III) showed the strongest absorption bands at 974, 670, and 460 cm^{-1} related to the internal tetrahedral vibrations found in all zeolites. The peaks at 974 and 670 cm^{-1} are attributed to the Si–O–Al asymmetric and symmetric stretching vibrations, respectively, while the band at 460 cm^{-1} corresponded to the TO$_4$ bending vibration. Moreover, the bands at 1082, 755, and 560 cm^{-1} were sensitive to the presence of external linkages between tetrahedra and the mode of arrangement of the zeolite secondary units, the peaks at 1082 and 755 being attributed to stretching modes and the signal at 560 being assigned to the presence of the double rings (Breck, 1974).

In relation to the IR spectra of zeolite A (Fig. 4b.IV and Fig. 4b.V), the structure analysis is quite similar to that described previously for zeolite X. Significant peaks were observed at ~1000, ~665, and ~463 cm^{-1} corresponding to the internal tetrahedral vibrations. The absorption bands related to external linkages were situated at 1096 and 557 cm^{-1}. The peak at 1096 cm^{-1} is related to asymmetric stretching modes. In this case, the absorption band at 557 cm^{-1} showed the presence of the four-membered double rings (D4R).

When comparing the FTIR signal positions of the structural zone of the volcanic ash with those of the zeolitized products, the peaks shifted to lower wavenumbers for zeolites A and X. The stretching modes are known to be sensitive to the Si:Al molar ratio present in the zeolite network. This fact could be attributed to the perturbation of the Si–O–Si stretching vibration by Al or strongly coupled Al–O in the AlO$_4$ tetrahedra and Si–O vibrations (Roy, 1990). The FTIR results corroborated the incorporation of Al in the network, which promoted the

Table 3. Type of zeolite obtained and maximum conversion percentage attained in the various synthesis products

Sample	Maximum conversion		Zeolite Type
	Reaction time (h)	%	
VA$_{CZ}$1	24	72	X
VA$_{CZ}$2	3	88	A
VA$_Z$1	3	–	P
	6	5	P + Tr A
VA$_Z$2	–	–	HS
VA$_{ZM}$	6	–	P
	24	6	P + Tr A
VA40$_{ZC}$1	6	21	A
VA40$_{ZC}$2	6	25	A
VA40$_{ZMC}$1	6	23	A
VA40$_{ZMC}$2	6	25	A

formation of the new aluminosilicate zeolitic structures at the expense of quartz, andesine, and the non-crystalline fraction belonging to volcanic ash.

Textural Properties

The activation and subsequent synthesis procedure allowed conversion of the macro-mesoporous structure of volcanic ash (50–500 Å according to IUPAC convention, Sing et al., 1985) with a very small surface area of 1.5 m^2·g^{-1}(Muñoz et al., 2019) into a microporous framework with enhanced surface-area values.

The N$_2$adsorption-desorption isotherm and the differential pore-size distribution were analyzed for sample VA$_{CZ}$1 (Fig. 5). In relation to the sodium form of LTA zeolite

sample (VA$_{CZ}$2), the data for nitrogen physisorption at 77 K were not acquired because the small pore size of NaA does not allow N$_2$ to enter at a measurable rate at 77 K, giving unrepresentative results (Du & Wu, 2007).

For the VA$_{CZ}$1 sample, according to IUPAC classification, a type I isotherm typical of microporous materials was observed (Fig. 5a). The BET specific surface area was 415 m^2·g^{-1}, where 361 m^2·g^{-1} and 54 m^2·g^{-1} corresponded to t-plot micropore area and t-plot external surface area, respectively. These values were on the order of those expected for a zeolite X. The total pore volume was 0.25 cm^3·g^{-1}, while the pore-size distribution showed a single peak centered at 2.36 nm (Fig. 5b), similar to the diameter of the supercage surrounded by ten sodalite units, which can be found in FAU structures. These results, together with those obtained from the XRD and FTIR techniques, confirmed the presence of zeolite X in the VA$_{CZ}$1 sample. Zeolite X (VA$_{CZ}$1) showed the absence of mesopores and an adsorption isotherm characteristic of a microporous material.

Morphological Analyses

Samples VA and VA40 obtained before and after pretreatments were analyzed by SEM. Samples VA and VA40 consisted of irregularly shaped particles with cavities of different sizes (Figs 6a and c, respectively). The crystalline morphologies appeared after alkaline treatment of VA$_C$(Fig. 6b) and VA40$_C$(Fig. 6d), both samples calcined for 12 h at 800°C with 50 wt.% Na$_2$CO$_3$.

The products obtained after synthesis were also studied by SEM (Fig. 7). Sample VA$_{ZC}$1, obtained after 24 h of reaction, clearly exhibited zeolite X crystals with a particle size of ~2–3 µm (Fig. 7a,b). After 3 h of reaction (VA$_{ZC}$2), zeolite A crystals of ~0.5–1 µm were observed (Fig. 7c,d). For sample VA$_{MZ}$, SEM images showed intergrowth of rounded and cubic crystal shapes of zeolites P and A (Fig. 7e). Rounded hydroxysodalite crystals of ~5–7 µm were formed in sample VA$_Z$2 (Fig. 7f).
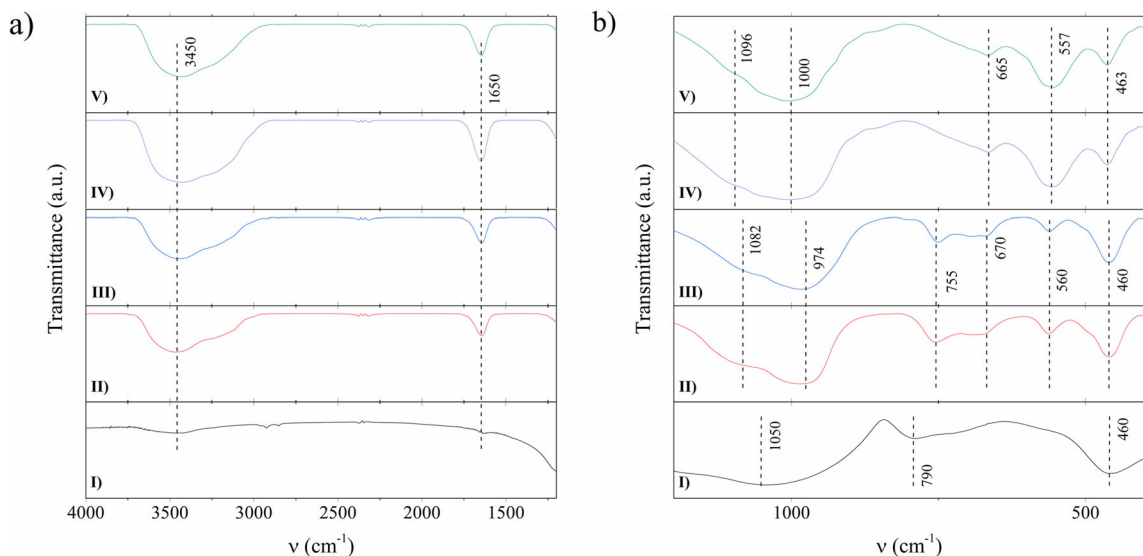
Fig. 4. FTIR spectra of samples **I** VA, **II** pure zeolite X, **III** VA$_{CZ}$1, **IV** pure zeolite A, and **V** VA$_{CZ}$2 in the **a**4000–1200 cm^{-1} range and **b**1200–400 cm^{-1} range

a)   b)
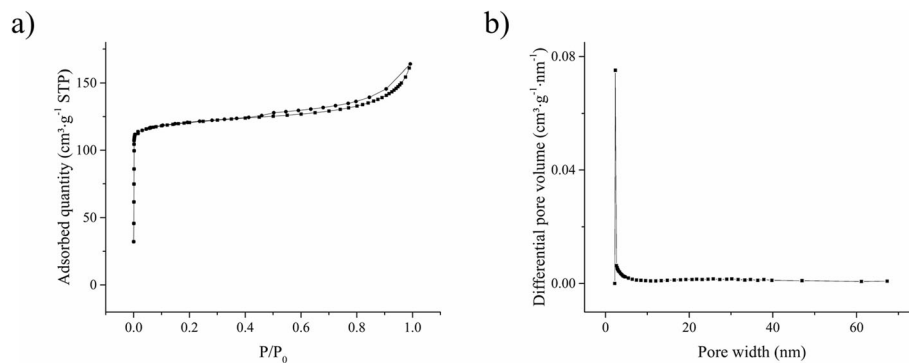
Fig. 5. a N_2 adsorption/desorption isotherm and **b** Horvath-Kawazoe differential pore-size distribution of $VA_{CZ}1$

CONCLUSIONS

Zeolites A and X were obtained successfully using volcanic ash as a raw material. The crystallinity of the ash, the application of adequate activation pretreatment, and the adjustment of reaction variables (batch composition and crystallization time) were required in order to obtain the best zeolitic structures.

Even under appropriate activation conditions, the mineralogical composition of the volcanic ash seemed to control the generation of polymorphs. The alkaline activation applied to crystalline samples led to the dissolution of quartz and plagioclase with the concomitant displacement of compensating ions, followed by the reorganization of Al and Si species into new $NaAlSiO_4$ polymorphs. The X-ray analysis corroborated the generation of low levels of nepheline and low-carnegieite from non-crystalline samples, including samples with an additional activation promoted by milling. The greater the contents of nepheline and low-carnegieite in the intermediate samples obtained after aging, the better the resulting conversions to
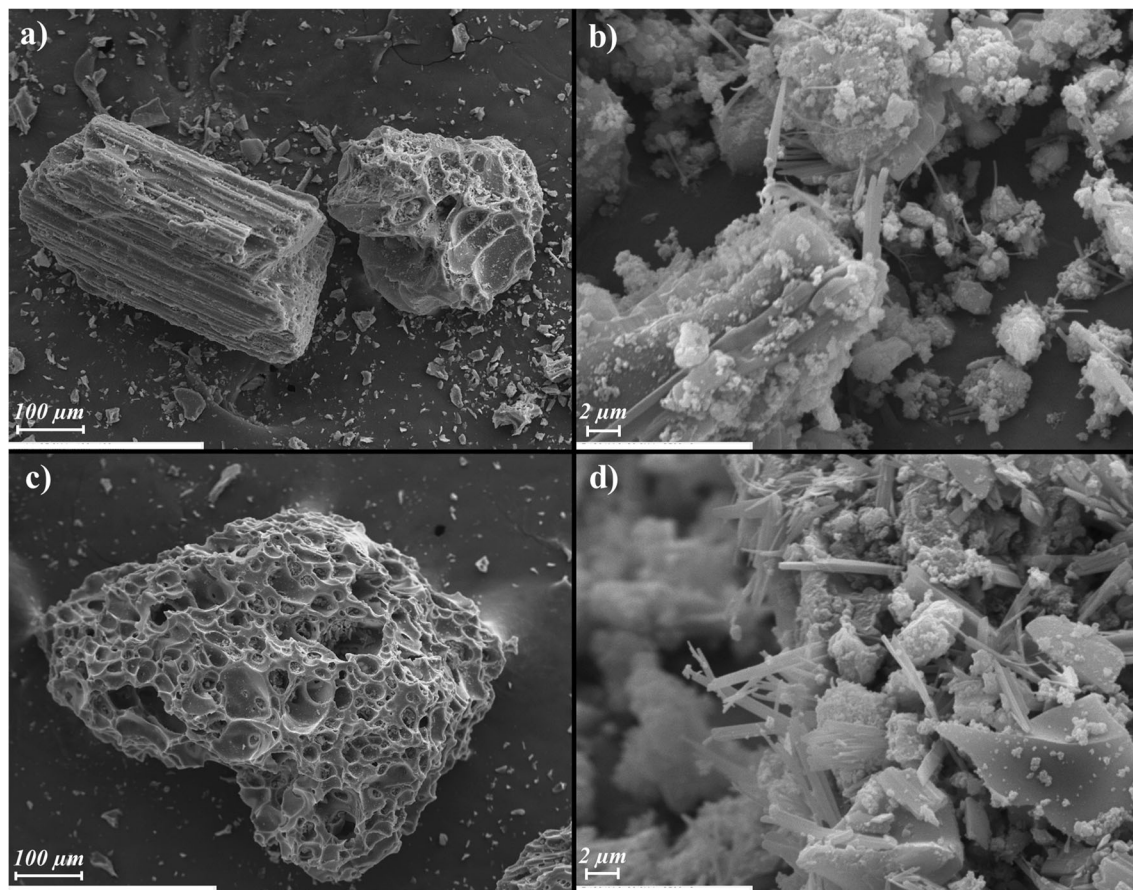
Fig. 6. Morphology of the volcanic ash samples before and after pretreatment: **a** natural VA, **b** VA_C, **c** VA40, and **d** $VA40_C$
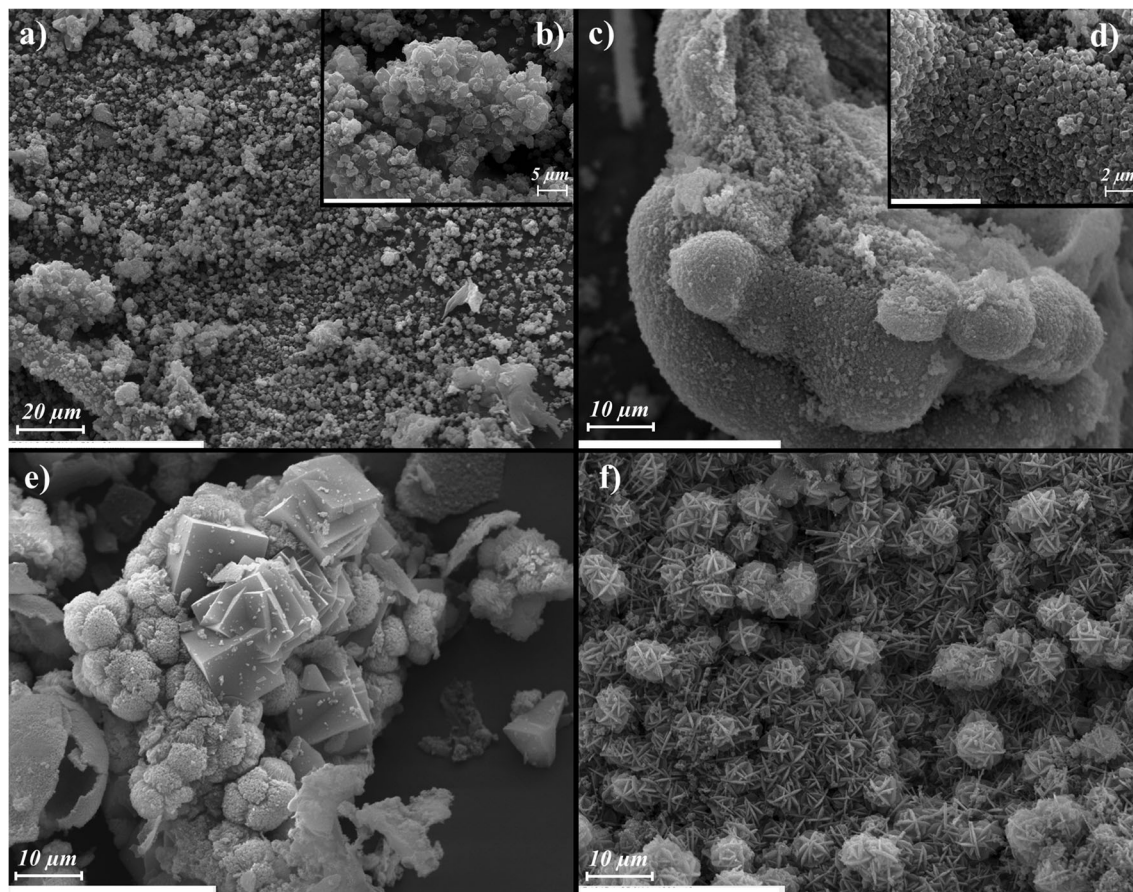
Fig. 7. Morphology of the synthesized products: **a** Zeolite X crystals in VA$_{ZC}$1 sample, **b** enlargement showing the surface covered by the crystals formed, **c** zeolite A crystals in VA$_{ZC}$2, **d** enlargement showing the surface covered by zeolite A, **e** zeolite P crystals found in VA$_{MZ}$, and **f** hydroxysodalite crystals in VA$_{MZ}$

zeolite A or X. On the other hand, samples without treatment generated zeolite P or hydroxysodalite, with remaining plagioclase. These conclusions are in accord with previous observations resulting from the conversion of aluminosiliceous wastes. The textural property results confirmed that ash activation and the subsequent synthesis procedure allowed conversion of a small-surface-area volcanic ash (BET area = 1.5 m^2 g^{-1}) into a microporous solid with an enhanced surface area of 415 m^2 g^{-1} (VACZ1). The results obtained show that, in hydrothermal conversion, the generation of an intermediate crystalline phase consisting of unstable polymorphic species undoubtedly promotes further zeolite growth, regardless of the starting aluminosiliceous source employed.

REFERENCES

Al-Fadala, S., Chakkamalayath, J., Al-Bahar, S., Al-Aibani, A., & Ahmed, S. (2017). Significance of performance based specifications in the qualification and characterization of blended cement using volcanic ash. *Construction and Building Materials, 144*, 532–540.

Baerlocher, C., McCusker, L. B., & Olson, D. H. (2007). *Atlas of Zeolite Framework Types*. Elsevier.

Belviso, C., Abdolrahimi, M., Peddis, D., Gagliano, E., Sgroi, M., Lettino, A., Roccaro, P., Vagliasindi, F. G. A., Falciglia, P. P., Di Bella, G., Giustra, M. G., & Cavalcante, F. (2021). Synthesis of zeolite from volcanic ash: Characterization and application for cesium removal. *Microporous and Mesoporous Materials, 319*, 111045.

Boscoboinik, J. A., Yang, X. Y. B., Shaikhutdinov, S., & Freund, H. J. (2013). Building blocks of zeolites on an aluminosilicate ultra-thin film. *Microporous and Mesoporous Materials, 165*, 158–162.

Botto, I. L., Canafoglia, M. E., Gazzoli, D., & González, M. J. (2013). Spectroscopic and microscopic characterization of volcanic ash from puyehue-(Chile) eruption: Preliminary approach for the application in the arsenic removal. *Journal of Spectroscopy*, 1–8. https://doi.org/10.1155/2013/254517

Breck, D. W. (1974). *Zeolite Molecular Sieves*. Wiley.

Brunauer, S., Emmett, P. H., & Teller, E. (1938). Adsorption of Gases in Multimolecular Layers. *Journal of the American Chemical Society, 60*, 309–319.

Canafoglia, M. E., Vasallo, M., Barone, V., & Botto, I. L. (2012). Problems associated to natural phenomena: potential effects of PCCVC eruption on the health and the environment in different zones of Villa La Angostura, Neuquén, Argentina. *AUGMDOMUS, 4*, 1–11.

Chen, L., Qian, J.-Y., Yang, C., Xu, P.-P., Zhu, D.-D., Zhong, J., et al. (2020). Direct synthesis of 5A zeolite from palygorskite: the influence of crystallization directing agent on the separation performance for hexane isomers. *Clays and Clay Minerals,68*, 1–8.

Collini, E., Osores, M. S., Folch, A., Viramonte, J. G., Villarosa, G., & Salmuni, G. (2013). Volcanic ash forecast during the June 2011 Cordón Caulle eruption. *Natural Hazards, 66*, 389–412.

Covey, J., Dominelli, L., Horwell, C. J., Rachmawati, L., Martin del Pozzo, A. L., Armienta, M. A., Nugroho, F., & Ogawa, R. (2021). Carers' perceptions of harm and the protective measures taken to safeguard children's health against inhalation of volcanic ash: A comparative study across Indonesia, Japan and Mexico. *International Journal of Disaster Risk Reduction, 59*, 102194.

Crundwell, F. K. (2014). The mechanism of dissolution of minerals in acidic and alkaline solutions: Part II Application of a new theory to silicates, aluminosilicates and quartz. *Hydrometallurgy, 149*, 265–275.

Dimitrijevic, R., Dondur, V., Vulic, P., Markovic, S., & Macura, S. (2004). Structural characterization of pure Na-nephelines synthesized by zeolite conversion route. *Journal of Physics and Chemistry of Solids, 65*, 1623–1633.

Du, X., & Wu, E. (2007). Porosity of microporous zeolites A, X and ZSM-5 studied by small angle X-ray scattering and nitrogen adsorption. *Journal of Physics and Chemistry of Solids, 68*, 1692–1699.

Elissondo, M., Baumann, V., Bonadonna, C., Pistolesi, M., Cioni, R., Bertagnini, A., Biass, S., Herrero, J. C., & Gonzalez, R. (2016). Chronology and impact of the 2011 Cordón Caulle eruption, Chile. *Natural Hazards and Earth System Sciences, 16*, 675–704.

Folch, A., Jorba, O., & Viramonte, J. (2008). Volcanic ash forecast - Application to the May 2008 Chaitén eruption. *Natural Hazards and Earth System Sciences, 8*, 927–940.

Gautam, P. K., Kalla, P., Jethoo, A. S., Agrawal, R., & Singh, H. (2018). Sustainable use of waste in flexible pavement: A review. *Construction and Building Materials, 180*, 239–253.

Gonzalez, M. R., Pereyra, A. M., Bosch, P., Fetter, G., Lara, F. V. H., & Basaldella, E. I. (2016). Structural and morphological evolutions of spent FCC catalyst pellets toward NaA zeolite. *Journal of Materials Science, 51*, 5061–5072.

Gougazeh, M., Kooli, F., & Buhl, J. C. (2019). Removal efficiency of basic blue 41 by three zeolites prepared from natural Jordanian kaolin. *Clays and Clay Minerals, 67*, 143–153.

Gregg, S. J., & Sing, K. S. W. (1982). *Adsorption Surface Area and Porosity*. Academic Press.

Hamilton, J. P., Brantley, S. L., Pantano, C. G., Criscenti, L. J., & Kubicki, J. D. (2001). Dissolution of nepheline, jadeite and albite glasses: Toward better models for aluminosilicate dissolution. *Geochimica et Cosmochimica Acta, 65*, 3683–3702.

He, X., Yao, B., Xia, Y., Huang, H., Gan, Y., & Zhang, W. (2020). Coal fly ash derived zeolite for highly efficient removal of Ni^{2+} in waste water. *Powder Technology, 367*, 40–46.

Horvath, G., & Kawazoe, K. (1983). Method for the calculation of effective pore size distribution in molecular sieve carbon. *Journal of Chemical Engineering of Japan, 16*, 470–475.

Jiménez-Alvarez, F. J., & Téllez-Jurado, L. (2010). Efecto de un aditivo plastificante comercial sobre la estructura cristalina de la plagioclasa utilizada en la fabricación de blocks ligeros de concreto. *Superficies y Vacío, 23*, 104–108.

Klüser, L., Erbertseder, T., & Meyer-Arnek, J. (2013). Observation of volcanic ash from Puyehue–Cordón Caulle with IASI. *Atmospheric Measurement Techniques, 6*, 35–46.

Kumar, A., Dhoble, S. J., Peshwe, D. R., & Bhatt, J. (2014). Structural and Photoluminescence properties of nepheline-structure $NaAlSiO_4:Dy^{3+}$ nanophosphors. *Journal of Alloys and Compounds, 609*, 100–106.

Lee, M. G., Park, J. W., Kam, S. K., & Lee, C. H. (2018). Synthesis of Na-A zeolite from Jeju Island scoria using fusion/hydrothermal method. *Chemosphere, 207*, 203–208.

Lemougna, P. N., MacKenzie, K. J. D., & Melo, U. F. C. (2011). Synthesis and thermal properties of inorganic polymers (geopolymers) for structural and refractory applications from volcanic ash. *Ceramics International, 37*, 3011–3018.

Lemougna, P. N., Wang, K.-T., Tang, Q., Nzeukou, A. N., Billong, N., Melo, U. C., & Min, C. X. (2018). Review on the use of volcanic ashes for engineering applications. *Resources, Conservation and Recycling, 137*, 177–190.

Loewenstein, W. (1954). The distribution of aluminum in the tetrahedra of silicates and aluminates. *American Mineralogist, 39*, 92–96.

Lutz, W., Engelhardt, G., Fichtner-Schmittler, H., Peuker, C., Löffler, E., & Siegel, H. (1985). The influence of water steam on the direct phase transformation of zeolite NaA to nepheline by thermal treatment. *Crystal Research and Technology, 20*, 1217–1223.

Mohamed, R. M., Mkhalid, I. A., & Barakat, M. A. (2015). Rice husk ash as a renewable source for the production of zeolite NaY and its characterization. *Arabian Journal of Chemistry, 8*, 48–53.

Monzón, J. D., Pereyra, A. M., Conconi, M. S., & Basaldella, E. I. (2017). Phase transformations during the zeolitization of fly ashes. *Journal of Environmental Chemical Engineering, 5*, 1548–1553.

Muñoz, M., Pasquale, G., Sathicq, A. G., Romanelli, G. P., Cabello, C. I., & Gazzoli, D. (2019). Volcanic ash as reusable catalyst in the green synthesis of 3H-1,5-benzodiazepines. *Green Processing and Synthesis, 8*, 600–610.

Rao, Y. J., & Murthy, I. S. N. (1974). Nepheline as a metasomatic product. *American Mineralogist, 59*, 690–693.

Rietveld, H. M. (1969). A profile refinement method for nuclear and magnetic structures. *Journal of Applied Crystallography, 2*, 65–71.

Rodríguez-Carvajal, J. (2001). Recent developments of the program FULLPROF, in commission on powder diffraction (IUCr). *Newsletter, 26*, 12–19.

Roy, B. N. (1990). Infrared spectroscopy of lead and alkaline-earth aluminosilicate glasses. *Journal of the American Ceramic Society, 73*, 846–855.

Sanhueza Núñez, V. M., & Bennun Torres, L. D. (2015). Synthesis of zeolitic materials from volcanic ash in presence and absence of cetyltrimethylammonium bromide. *Revista Internacional de Contaminación Ambiental, 31*, 185–193.

Siddique, R. (2011). Effect of volcanic ash on the properties of cement paste and mortar. *Resources, Conservation and Recycling, 56*, 66–70.

Sing, K. S. W., Everett, D. H., Haul, R. A. W., Moscou, L., Pierotti, R. A., Rouquérol, J., & Siemieniewska, T. (1985). Reporting physisorption data for gas/solid systems with special reference to the determination of surface area and porosity (Recommendations 1984). *Pure Applied Chemistry, 57*, 603–619.

Tait, K. T., Sokolova, E., Hawthorne, F. C., & Khomyakov, A. P. (2003). The crystal chemistry of Nepheline. *The Canadian Mineralogist, 41*, 61–70.

Tchakoute, H. K., Elimbi, A., Yanne, E., & Djangang, C. N. (2013). Utilization of volcanic ashes for the production of geopolymers cured at ambient temperature. *Cement and Concrete Composites, 38*, 75–81.

Tchakoute Kouamo, H., Elimbi, A., Mbey, J. A., Ngally Sabouang, C. J., & Njopwouo, D. (2012). The effect of adding alumina-oxide to

metakaolin and volcanic ash on geopolymer products: A comparative study. *Construction and Building Materials, 35*, 960–969.

Upadhyay, D. (2012). Alteration of plagioclase to nepheline in the Khariar alkaline complex, SE India: Constraints on metasomatic replacement reaction mechanisms. *Lithos, 155*, 19–29.

Wilson, T. M., Cole, J. W., Stewart, C., Cronin, S. J., & Johnston, D. M. (2011). Ash storms: impacts of wind-remobilised volcanic ash on rural communities and agriculture following the 1991 Hudson eruption, southern Patagonia, Chile. *Bulletin of Volcanology, 73*, 223–239.

Yamada, H., Sukenaga, S., Ohara, K., Anand, C., Ando, M., Shibata, H., Okubo, T., & Wakihara, T. (2018). Comparative study of aluminosilicate glass and zeolite precursors in terms of Na environment and network structure. *Microporous and Mesoporous Materials, 271*, 33–40.